Cement and Concrete Research 40 (2010) 1507–1516

Contents lists available at ScienceDirect

Cement and Concrete Research

journal homepage: http://ees.elsevier.com/CEMCON/default.asp

Laboratory investigation of reinforcement corrosion initiation and chloride threshold content for self-compacting concrete

Hui Yu [a,*], Xianming Shi [b,c], William H. Hartt [d], Baotong Lu [a]

[a] Materials Engineering Department, Southwest Research Institute®, 6220 Culebra Road, San Antonio, TX 78238, USA
[b] Corrosion and Sustainable Infrastructure Laboratory, Western Transportation Institute, Box 174250, College of Engineering, Montana State University, Bozeman, MT 59717-4250, USA
[c] Civil Engineering Department, 205 Cobleigh Hall, Montana State University, Bozeman, MT 59717-2220, USA
[d] Center for Marine Materials, Florida Atlantic University–Sea Tech Campus, 101 North Beach Road, Dania Beach, Florida 33004, USA

ARTICLE INFO

Article history:
Received 17 November 2009
Accepted 8 June 2010

Keywords:
Reinforcement (D)
Corrosion (C)
Chloride (D)
Concrete (E)
Reinforcing steel bar
Weibull distribution

ABSTRACT

Time-to-corrosion (T_i) of reinforcement in concrete and chloride threshold content (C_{th}) are important service life determinants for reinforced concrete structures in chloride-laden environments. In this study, the two determinants of a series of self-compacting concretes (SCC) and regular concretes were experimentally investigated. A new sampling approach for C_{th} determination (milling powder from corrosion active site at the rebar/concrete interface) was adopted to accurately express chloride content resulting in corrosion occurrence. It is found that the T_i and C_{th} follow the 3-parameter Weibull distribution. The results indicate that the corrosion initiation of rebar in concrete slabs depends upon both cement alkalinity and superplasticizer. Rebar, embedded in high alkalinity cement SCC, exhibits better corrosion resistance as indicated by the longer T_i, higher C_{th} and larger Weibull modulus, m. A larger Weibull modulus indicates that anti-corrosion performance of rebar in slabs is more stable and less scattered. The effects of specific superplasticizer on rebar corrosion resistance are discussed from the viewpoint of air void amount and size distribution at the rebar/concrete interface.

1. Introduction

Corrosion of reinforcing steel bar (rebar) due to chloride ingress is one of the major mechanisms leading to the premature degradation of concrete structures such as highway bridges. It causes immense economic loss and safety implications [1–3]. Chlorides, from either marine environments or deicing salt applications, can compromise rebar passivity and initiate active corrosion once the Cl^- content at rebar depth reaches a threshold level (C_{th}). The time it takes for chlorides to reach this C_{th}, defined as time-to-corrosion, T_i, is the most critical factor in determining the resistance of reinforced concrete to the chloride-laden environment. Therefore, both C_{th} and T_i are important service life determinants for reinforced concrete structures [4,5].

Numerous studies [6–16] have been conducted and reported, with experimental or modeling approaches (or both), that these two determinants can change as a function of cement type, reinforcement type, mix design, exposure conditions, etc. Nonetheless, all these studies are limited to conventional Portland cement concrete (PCC) and there has been little research focused on the corrosion initiation of rebars in self-compacting concrete (SCC). In recent years, SCC has gained popularity with the construction industry, as it features improved placeability of fresh concrete and thus eliminates the need for noisy, energy-consuming compaction or for concrete mixes with a high water-to-cementitious-material ratio. SCC, generally achieved by admixing superplasticizer into concrete mix, is a desirable alternative to PCC, particularly in construction projects where compaction is difficult to achieve. Therefore, it is necessary to understand the corrosion performance of rebar in SCC, especially the impact of superplasticizer addition.

A wide range of C_{th} and T_i values have been reported for corrosion initiation of rebar in PCC, owing to the probabilistic nature of rebar corrosion initiation as well as the variability of chloride exposure conditions. Glass et al. [17] and Alonso et al. [18,19] summarized historical literature and noted that C_{th} values spread over more than one order of magnitude. The complexity inherent in C_{th} and T_i is that they are affected by a number of factors interdependently. It is believed that the following variables ultimately define these two determinants: 1) type of raw materials (especially cement composition) and admixtures; 2) mix design (especially water-to-cement ratio, w/c); 3) execution and curing circumstances; 4) type of steel bar (hot-rolled, hot-rolled micro-alloyed, temperature, work-hardened etc.); 5) rebar surface condition; 6) exposure conditions; and 7) sampling method for chloride analysis [20]. Another factor contributing to the complexity is the approach employed to determine T_i. Currently, even though there are several electrochemical methods,

* Corresponding author. Tel.: +1 210 522 5728; fax: +1 210 522 5122.
E-mail address: hui.yu@swri.org (H. Yu).

0008-8846/$ – see front matter © 2010 Elsevier Ltd. All rights reserved.
doi:10.1016/j.cemconres.2010.06.004

e.g., polarization resistance and electrochemical impendence (EIS) are available for laboratory and field practice, half-cell potential coupled with macro-cell current measurement is the most popular approach and has been standardized [21] for T_i determination.

Recently, the physical condition of rebar/concrete interface (especially entrapped air void content) was found to be more influential for C_{th} than the chloride binding or buffering capacity of cement paste matrix [16]. Laboratory observation shows that even for seemingly identical concrete slabs, variability of C_{th} and T_i is introduced by micro-structural factors such as the size and distribution of entrapped air voids, and the arrangement of aggregates which can significantly affect the tortuosity of chloride ingress path [22]. Monfore and Verbeck [23] reported a correlation between entrapped air voids and sites of corrosion initiation, but only limited efforts have subsequently focused on this topic. At the rebar/concrete interface, the sites with entrapped air voids feature the absence of hydration products and allow easy access for dissolved oxygen and free chlorides. As such, an increasing air void content at the interface leads to a greater probability of lower C_{th} [16]. Further, Söylev and Francois [24] argued that at the rebar/concrete interface macro-defects have a direct impact on corrosion whereas micro-defects have no significant effect. Macro-defects herein imply large air voids and/or gaps formed beneath the horizontal reinforcement as a result of bleeding and settlement of fresh concrete.

The method that has been used to determine the chloride content or its profile in concrete certainly contributed to the variability in reported C_{th} values. Traditionally, both the chloride content profile in concrete and the C_{th} value are determined using the coring method, which involves acquisition of one or more cores from sound concrete between reinforcements at the time of active corrosion initiation. The cores are sliced and analyzed for their chloride content, and the chloride content in the slice corresponding to the reinforcement cover is defined as C_{th}. Recently, both experimental [20,25–29] and modeling [30–34] studies revealed that chloride content at the top of the rebar is higher than that at the same depth away from the rebar. This was explained by the relatively low content of coarse aggregates in the vicinity of the rebar [22] as well as the rebar serving as a physical barrier to chloride migration [26,27].

In addition, the probabilistic nature of local corrosion is an important factor resulting in scattered C_{th} and T_i values. Hartt and Nam [25] reported a range of values for C_{th} and T_i with seemingly identical slabs and the same exposure condition. The results indicate that these two service life determinants should be represented by a probability function instead of a specific value. However, there is limited research on the probabilistic nature of how mix design and other factors impact corrosion initiation (as indicated by C_{th} and T_i), especially when applied to SCC [28,29]. A statistical approach that can effectively characterize T_i and C_{th} and assess the corrosion initiation risk in SCC is thus much needed.

The aim of this study was to investigate and discuss the probabilistic nature of rebar T_i and C_{th} in SCC, with regular PCC slabs as control. Air voids at the rebar/concrete interface have also been analyzed, in light of their potential impact on the variability of T_i and C_{th} in SCC.

2. Experimental

In this study, a series of ASTM G109 [35] type (schematics of which are shown in Fig. 1) SCC and regular PCC slabs were cyclically exposed to chloride solutions and continuously monitored for corrosion potential and macro-cell current in order to determine T_i. Subsequent to corrosion initiation, the slabs were dissected and the chloride content was determined from titration results of milled concrete powder acquired from both corrosion active and passive sites atop of rebar. The amount and size distribution of air voids at the rebar/concrete interface were also analyzed to facilitate explanation of the abovementioned experiment results.

2.1. Materials

Two kinds of type I Portland cement were employed to cast the reinforced concrete slabs, with composition listed in Table 1. The equivalent alkalinity (Na_2O-equivalent) of each was determined from the following expression,

$$Na_2O\text{—}equivalent = Na_2O(\text{wt.\%}) + 0.658 \times K_2O(\text{wt.\%}). \quad (1)$$

As such, the Na_2O-equivalent was calculated to be 0.39% and 1.14% with the former designated as NA (normal alkalinity) and the latter HA (high alkalinity). These same designations (NA, HA) were used to identify individual slabs according to the employed cement type. Physical characteristics of both coarse and fine aggregates used to fabricate the concrete slabs are provided in Table 2. Rebars used for this study were of Grade #5 carbon steel, with a nominal diameter of 15.9 mm (0.625 in.). A commercial high-range water reducing admixture (superplasticizer), PLASTOL 5000, manufactured by Euclid Chemical (Cleveland, OH), was used to improve the flowability and placeability of fresh SCC batches.

2.2. Slab preparation

The procedures of concrete slab fabrication and rebar preparation followed ASTM G109 [35]. When the concrete batches were ready,

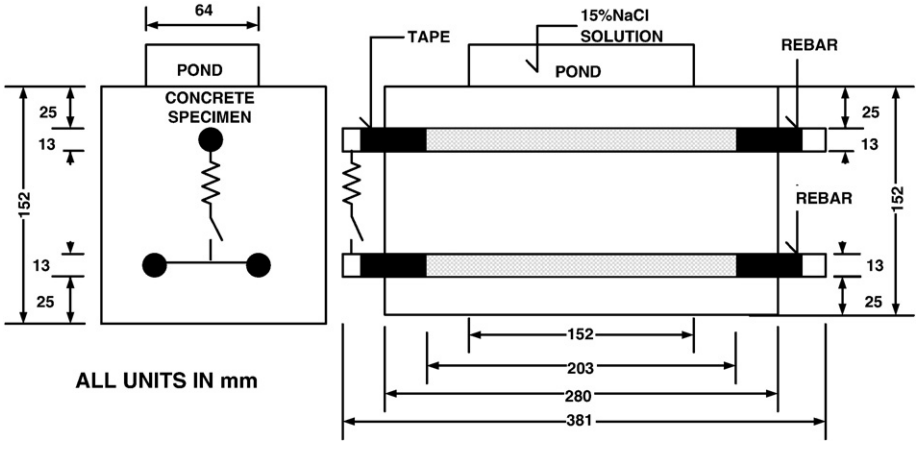

Fig. 1. Schematics of ASTM G109 slab geometry.

Table 1
Chemical composition of normal alkalinity (NA) and high alkalinity (HA) cements.

Chemical composition	SiO_2, %	Al_2O_3, %	Fe_2O_3, %	CaO, %	MgO, %	SO_3, %	Na_2O, %
NA, Cemex, Brooksville, type I	21.66	4.82	3.8	63.53	0.68	2.97	0.08
HA, St Mary's Detroit, MI	20.08	4.95	3.05	61.98	2.52	4.2	0.278
	K_2O, %	TiO_2, %	P_2O_5, %	Mn_2O_3, %	SrO, %	F, %	Cr_2O_3, %
NA, Cemex, Brooksville, type I	0.47	0.29	0.081	0.049	0.06	0.052	0.002
HA, St Mary's Detroit, MI	1.15	0.26	0.178	0.074	0.09	0.057	0.002

seven duplicate slabs were fabricated for each set. Six slabs were used for exposure to chlorides and the remaining one was used for characterizing the air voids at the rebar/concrete interface. Table 3 tabulates mix design and properties of the concrete batches. The slabs were poured with the molds upside-down relative to slab orientation during exposure. As such, there was a greater risk of air voids caused by air bubbles and bleeding forming at the top rebar surface relative to the bottom.

Concrete batch nomenclature: SCC50NA and SCC50HA are the 0.5 *w/c*, normal and high alkalinity SCC slabs, respectively. 50NAR and 50HAR are the 0.5 *w/c*, normal and high alkalinities, regular concrete slabs, respectively.

2.3. Slab exposure and monitoring

Prior to being cured in a moist room (relative humidity approximately 90%) for 28 days, the slabs were kept in molds for 24 h after cast. Subsequently, chloride exposure for all the slabs started, following a one-week wet and one-week dry ponding cycle. To compensate for water loss during the process of epoxy coating etc. in the relatively dry environment, ponding cycles were built up carefully. Distilled water was used for ponding in the first two cycles, followed by 3% NaCl solution cycle ponding in the next two cycles, and 9% NaCl solution cycle ponding in the two cycles thereafter. Subsequently, 15% NaCl solution cycle ponding was employed until active corrosion of the top rebar commenced.

In this study, T_i was determined by monitoring of the top rebar potential and macro-cell current flowing between the top and bottom rebars. Measurements were taken at the end of each wetting/drying cycle to indicate whether the top rebar was in a passive or active state. In the beginning, active corrosion was defined as having commenced if, for two consecutive data acquisition periods, the macro-cell current was 10 μA or greater, or the electrochemical potential for the top bar was −280 mV vs. Saturated Camel Electrode (SCE) or more negative [21]. Thereafter, the activated slab was dissected for visual examination of corrosion sites and chloride analysis. Please note that the potential difference between the top and bottom bars, the IR drop, initially was very low. Therefore, the measured potential differences are considered predominantly as a result of the corrosion of the top bar.

The first several dissected slabs indicated that the abovementioned criterion was too conservative to define corrosion initiation since these top rebars had one or more pronounced corrosion spots observed on their surface and large areas of rust at the rebar/concrete interface (as shown in Fig. 2a). Subsequently, the corrosion initiation criterion was adjusted to be that the macro-cell current was measurable (>0.1 μA) or the corrosion potential for the top bar was −100 mV (vs. SCE) or more negative for two consecutive data acquisition periods. Visual observation revealed small corrosion spots on the top rebar (as shown in Fig. 2b), which suggests that corrosion had just initiated. For the slabs dissected according to the 10 μA/−280 mV_{SCE} criterion, the T_i values were tracked back to the date when it met the revised criterion. Since the two criteria led to less than 10% difference in T_i, the chloride content values were assumed to be approximately the same, since no back calculation for the chloride contents in these slabs was feasible.

2.4. Slab autopsy

The exposure of individual slabs was terminated once active corrosion was determined. Slabs were then cut along the plane of the top bar on both longitudinal sides using a hand power-saw with diamond-cutting blade. After cutting, the slabs were opened by tapping along the saw cut with a chisel and hammer. To further confirm corrosion occurrence and adopted corrosion criterion, the sign of corrosion products on rebar was checked by visual inspection and recorded using a digital camera. The photograph in Fig. 2 illustrates the corrosion sign on rebar surface and corrosion products at the rebar/concrete interface. Also indicated in Fig. 2 are nominal corrosion active site and passive sites. In most cases, the dissection of the slabs was performed within a few days after active corrosion occurred and in limited cases within a week. This period is much shorter than the overall test duration (the time-to-open). Therefore, the electro-migration of chloride from the passive sites to the active sites in this short period can be neglected and the acquired chloride contents are roughly considered as chloride content at T_i.

2.5. Chloride content determination

In this study, milling of concrete along the top of the upper bar was employed to obtain powder samples for chloride analysis. Each concrete slab was first dissected and fractured along the plane of the top mat and its upper portion was then placed inverted in a mill. A cutter pass was made approximately 0.6 mm deep into the concrete along the top of the rebar trace where the steel remained passive. The acquired powder was for chloride content analysis at the passive site. At active corrosion sites (sites where corrosion products were seen), which were relatively small, concrete powder was milled and collected from an area approximately 0.6 mm deep and 5 mm wide. For each dissected slab, the concrete powder samples were individually analyzed for chloride content following the Florida Department of Transportation (FDOT) wet acid soluble method [36]. Note that the sampling process and chloride content analysis were conducted immediately after slab dissection.

The chloride content profile along the rebar/concrete interface length of slab SCC50HA#1 was also analyzed using an energy-dispersive x-ray (EDX) spectroscope (manufactured by Oxford Inc.), which had a resolution of 5 eV per channel and a scan range of 0–10 keV. The surface composition was analyzed using the INCA software. It is worthy to note that, for data from EDX, the chloride content is the atomic weight percent of all possible elements; whereas, chloride content data from

Table 2
Material type and physical properties of coarse and fine aggregates.

Properties	Material type	Specific gravity (surface saturated dry)	Saturated gravity (dry bulk)	Absorption (%)	Fineness modulus	Fineness modulus (standard derivation)	Sand equivalent
Coarse aggregate	Olitic limerock (Florida Limestone)	2.426	2.349	3.26	–	–	–
Fine aggregate	Silica sand	–	–	–	2.22	0.05	100

Table 3
Mix design and physical prosperities of the concrete batches.

Batch#	Cement alkali	*w/c*	Cement kg/m^3	Water kg/m^3	Sand kg/m^3	Stone kg/m^3	Superplasticizer ml	Slump cm	Spread cm	Air content %
SCC50NA	0.4	0.5	367.8	183.9	1004.6	732.2	101.8	20.6	66.0	7.6
50NAR	0.4	0.5	367.8	183.9	1004.6	732.2		22.9	35.6	3.1
SCC50HA	1.1	0.5	367.8	183.9	1004.6	732.2	119.7	26.7	64.8	6.6
50HAR	1.1	0.5	367.8	183.9	1004.6	732.2		12.7	24.1	3.3

wet acid soluble method [36] is based on chloride content per mass of concrete.

2.6. Air void analysis

For the slabs dissected immediately after curing (without exposure to chloride solutions), the air void amount and size distribution at the top half bar trace were analyzed, as described below. Depending on the shape, the voids were treated as either half sphere or ellipse. In the latter case, the void diameter was defined as one-half the sum of the length of the major and minor axes. A caliper was used for void size measurement. Only air voids no smaller than 0.1 mm (in diameter) were counted with naked eyes assisted by an optical microscope with magnification up to 5 times. All air voids equal to or smaller than 0.5 mm in diameter were counted as 0.5 mm in diameter. Similarly, larger air voids were counted and sorted in 0.50-mm increments. Fig. 3 schematically describes the method for measuring and calculating the air void diameter and Fig. 4 shows an example photograph with air voids at rebar trace. Please note that no analysis was performed to directly correlate air void to corrosion active site.

3. Results and discussion

3.1. Distribution of time-to-corrosion

Figs. 5–8 display the potential and macro-cell current as a function of exposure time for four sets of slabs respectively. Five of the six SCC50NA and SCC50HA slabs became active (corrosion initiated at the top bar) whereas all six of the 50NAR and 50HAR slabs became active. For active slabs, there was no clear correlation between the varying potential and macro-cell current data after corrosion initiated. Nevertheless, for most cases, the more abruptly the potential drop at corrosion initiation, the greater the macro-cell current.

The data of time-to-corrosion of the slabs, T_i, were experimentally determined and are summarized in Table 4. We can see that T_i in each group is highly scattered. As such, the T_i can be treated as a random variable because it is affected by the diverse factors mentioned in the introduction section.

When the chloride is accumulated at the rebar/concrete interface with increasing exposure duration, the corrosion will initiate at the weakest point(s) of the interface. This kind of problem can be dealt with the weakest link theory developed by Weibull [37]. The Weibull treatment of failure is in two parts: (1) a weakest link argument leading to size dependence for the distribution of corrosion resistance and (2) the assumption of a particular statistical distribution function [38]. The size may be volume, area or length, depending on the problem addressed. In the present study, since corrosion occurs on the interface of rebar/concrete, the size is defined as the area of interface. The weakest link argument is based on the idea that failure at any flaw leads to total failure and the interface is homogeneous in the sense that the flaws are distributed throughout the interface. Assume that the total area of the rebar/concrete interface exposed to the environment containing chloride with a concentration C at the moment T is A and divide it into a very large number of elements n of equal size ΔA. Take $P_{f,i}(T, \Delta A)$ as the probability of failure from the ith area element by a concentration C at the moment T. The probability that this element survives is therefore $1-P_{f,i}(T, \Delta A)$. Since the chloride concentration is taken to be the same for all area elements and the interface is assumed to be homogeneous, all $P_{f,i}(T, \Delta A)$ can be taken the same, $P_{f,i}(T, \Delta A)$. For the entire interface to survive the corrosive environment, all the surface elements must survive so that the total probability of survival, $1-P_f(T, A)$, of an interface $A = n\Delta A$ under a homogeneous environment is given by [38]

$$1-P_f(T,A) = [1-P_f(T,\Delta A)]^n = \left[1-\frac{A}{n}\frac{P_f(T\Delta A)}{\Delta A}\right]^n = \left[1-\frac{A}{n}\varphi(T)\right]^n \quad (2)$$

where we have assumed that as n increases $P_{f,i}(C, \Delta A)/\Delta A$ approaches a limit $\varphi(C)$. As the interface is subdivided into larger numbers of smaller elements, n approaches infinity and ΔA approaches zero. Then

$$\lim_{n\to\infty}\left(1-\frac{x}{n}\right)^n = \exp(-x) \quad (3)$$

So that

$$P_f(T,A) = 1-\exp[-A\varphi(T)]. \quad (4)$$

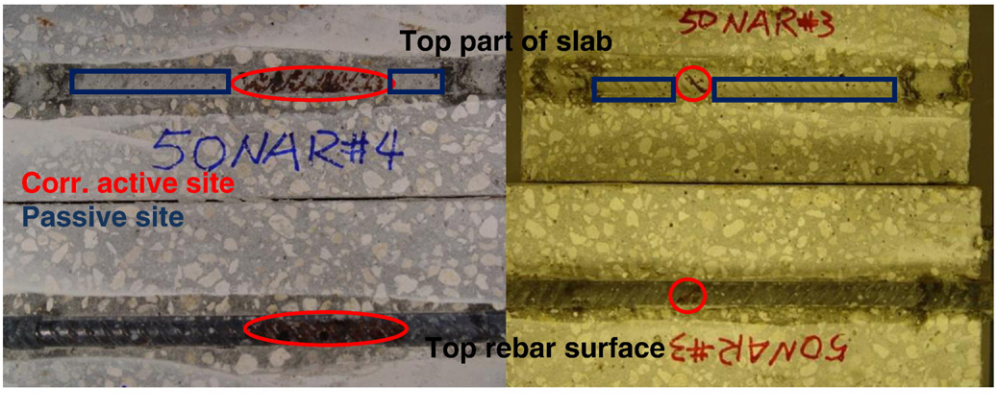

Fig. 2. Example photograph illustration of autopsied slabs with rebar corroded.

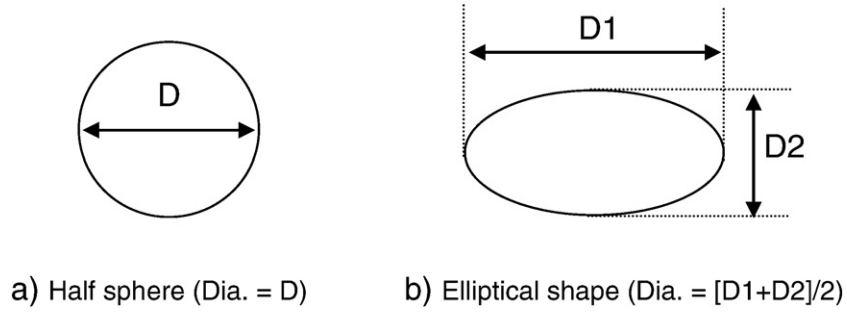

Fig. 3. Schematic description of air void diameter measurement.

This argument shows that the probability of failure of the rebar depends exponentially on the interface area times a risk function $\varphi(T)$ that characterizes the chloride content-dependence of cumulative failure probability per unit area at the limit of small area. This weakest link argument does not give a specific form for $\varphi(\sigma)$, but clearly it must be a monotonically increasing function of T. Weibull [37] assumed the form

$$\varphi(T) = [(T-T_0)/\sum_0]^m. \quad (5)$$

In Eq. (5), T_0 is the threshold exposure duration to initiate corrosion (before which $P_f = 0$). This gives the probability of failure of the rebar, P_f, as

$$P_f = 1-\exp\left[A\left(\frac{T-T_0}{\sum_0}\right)^n\right]. \quad (6)$$

Eq. (6) is the three-parameter Weibull distribution with the scale parameter,

$$T_c = \sum_0 A^{-\frac{1}{m}}. \quad (7)$$

In order to determine the threshold T_0 and Weibull modulus, m, the cumulative probability P_f in Eq. (2) was estimated with the empirical Eq. (8),

$$P_f = \frac{i-0.3}{k+0.4} \quad (8)$$

where, k is the total number of active slabs in each set and i represents the ith active slab in that set. Eq. (6) can thus be transformed into the following:

$$\ln(-\ln(1-P_f)) = m \times \ln(T-T_0). \quad (9)$$

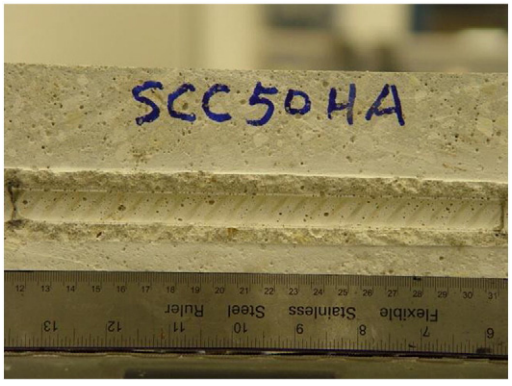

Fig. 4. An example photograph illustrates air voids at rebar trace.

Accordingly, $\ln(-\ln(1-P_f))$ vs. $\ln(T-T_0)$ would be a straight line with a slope of Weibull modulus, m, as shown by the data in Fig. 9. The values of T_0 and m for each group of slabs were determined from the test data utilizing the trial-and-error method while the correlation coefficient of the least-squares fitting curves is maximized.

The mean T_i, T_0 and m for each slab set are summarized in Table 4 and Fig. 10. The order of mean T_i is: SCC50HA> 50HAR>SCC50NA>50NAR and that of T_0 is: SCC50HA>50HAR>50NAR>SCC50NA. For mean T_i, rebar in slabs with high alkalinity cement, SCC50HA and 50HAR, are 3.9 and 3.6 times as long as that for the corresponding rebar in slabs with normal alkalinity, SCC50NA and 50NAR, respectively; for T_0, this discrepancy is 8.33 and 2.56 times respectively. These results demonstrate that the rebar embedded in slabs made with high alkalinity cement had much better resistance to chloride-induced corrosion and extended T_i than that in slabs made with normal alkalinity cement.

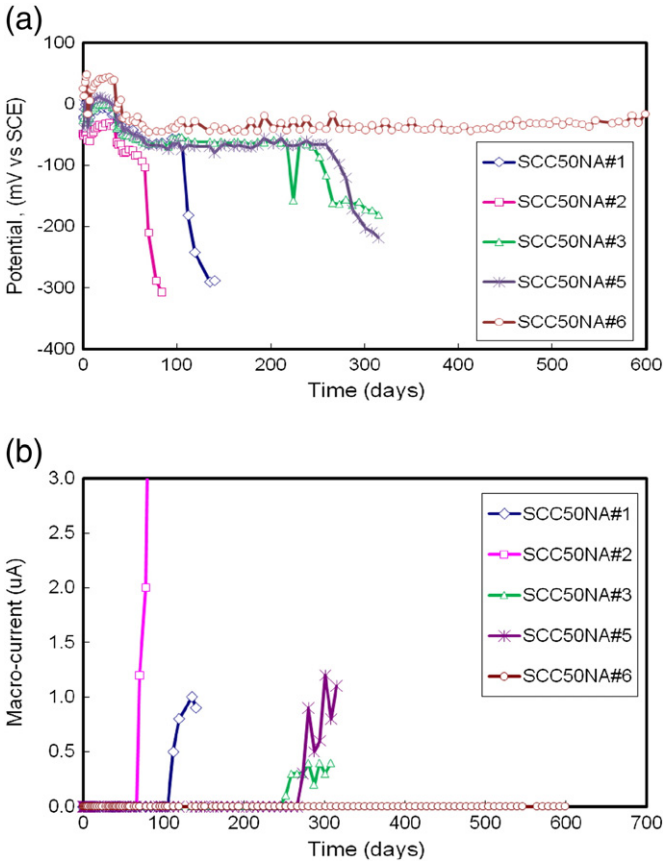

Fig. 5. Evolution of (a) potential and (b) macro-cell current over time for five G109 SCC50NA slabs.

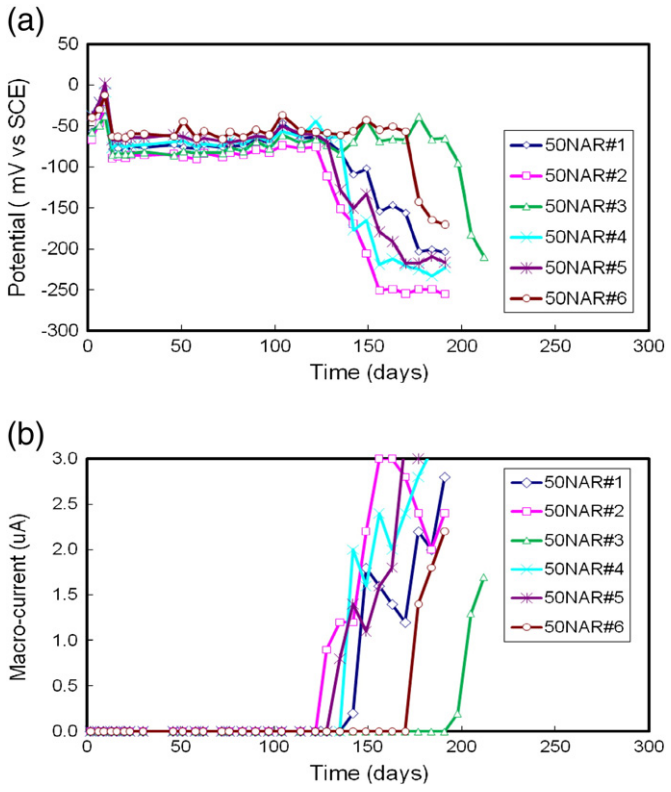

Fig. 6. Evolution of (a) potential and (b) macro-cell current over time for six G109 50NAR slabs.

Simultaneously, higher Weibull modulus, m, acquired for rebar in slabs with high alkalinity cement indicates that a small scatter of T_i. Similar phenomenon was also reported in literature [25]. This suggests that concrete made with high alkalinity cement featured more consistency concrete microstructure at the rebar/concrete interface, relative to concrete made with normal alkalinity cement.

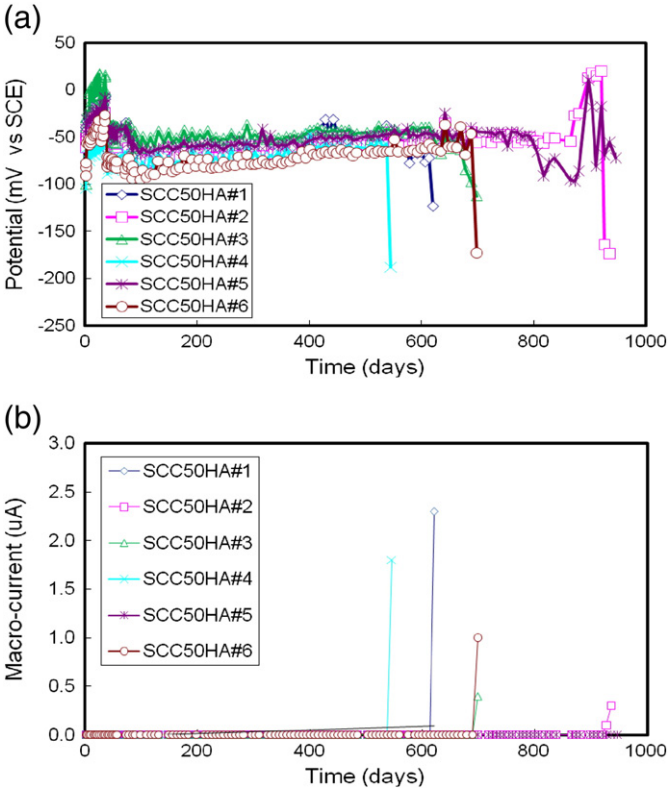

Fig. 7. Evolution of (a) potential and (b) macro-cell current over time for six G109 SCC50HA slabs.

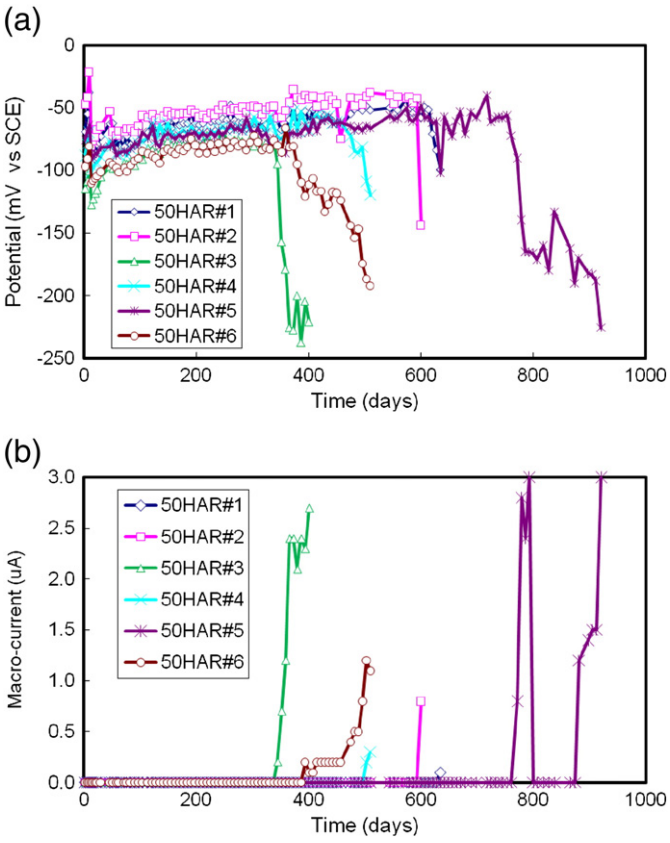

Fig. 8. Evolution of (a) potential and (b) macro-cell current over time for six G109 50HAR slabs.

Table 4
Experimental and analytical results.

Batch No.	ID	T_i, days	Mean T_i (T_m), days	T_0, days	m	Chloride content at passive site, kg/m^3	Chloride content at corr. active site, kg/m^3
50NAR	#1[a]	142	154	125	0.9011	1.51	2.14
	#2[a]	128				1.89	2.48
	#3	198				2.78	3.52
	#4[a]	142				1.51	2.54
	#5[a]	135				2.42	3.06
	#6	177				2.42	3.06
SCC50NA	#1[a]	112	179	60	0.7194	1.18	1.40
	#2[a]	70				0.79	1.02
	#3	259				4.25	5.50
	#4	–[b]				–	–
	#5	273				3.12	3.50
	#6	–[c]				–	–
50HAR	#1	635	551	320	0.9577	4.52	10.86
	#2	600				–	–
	#3	345				2.56	3.13
	#4	503				3.55	3.80
	#5	772				4.93	5.38
	#6	394				3.20	5.40
SCC50HA	#1	621	698	500	1.2272	4.07	5.65
	#2	927				5.12	6.48
	#3	699				4.98	6.14
	#4	545				4.21	6.56
	#5	–[c]				–	–
	#6	699				5.20	7.10

[a] The chloride content was not tracked back to T_i.
[b] There were significant defects on the slab surface and data was deleted.
[c] Slabs where the top bar had not corroded.

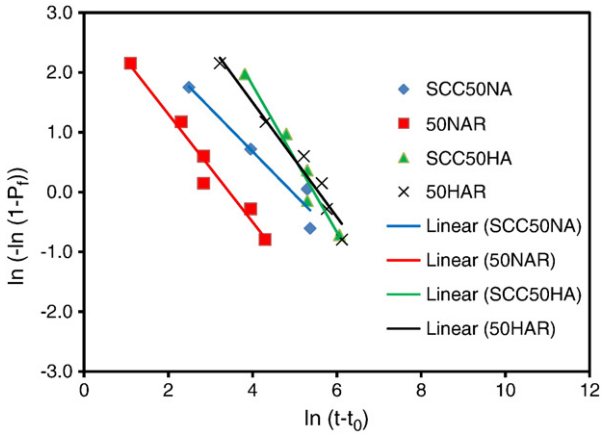

Fig. 9. T_i Weibull distribution plot for each mix set.

Addition of specific superplasticizer in mix batch with high alkalinity cement further improved the corrosion resistance of rebar in concrete. This is supported by the fact that the values of mean T_i, T_0, and m were all higher, 1.3, 1.6 and 1.3 times respectively, for SCC50HA than that for 50HAR. The better corrosion resistance of SCC50HA can be attributed to the improved workability and flowability of the fresh SCC concrete, as indicated by the higher slump and spread values relative to the conventional concrete mixes (shown in Table 3). Another factor to consider is the effect of superplasticizer addition on the amount and size distribution of air voids at the rebar/concrete interface, which will be discussed later.

In the case of concrete mixes with normal alkalinity cement, however, SCC50NA had higher mean T_i but lower T_0 and m values than 50NAR, implying the negative impacts of superplasticizer addition in normal alkalinity cement on rebar resistance to corrosion. The actual discrepancies should be greater than those shown in Table 4 because there was one more rebar in SCC slab that had not shown active corrosion until end of the experiments. The actual Weibull modulus (or the slope of the Weibull plot) would be even smaller, and the mean T_i be greater and T_0 be less for the SCC slabs. In the viewpoint of reliability, the SCC slabs with the normal alkalinity cement showed a higher risk for earlier corrosion initiation, implying that the specific superplasticizer to be utilized in concrete should be carefully selected. Higher air content (7.6%) and much more air voids at the rebar/concrete interface of normal alkalinity cement SCC slabs might have played a more negative role on this reduced corrosion resistance, which will be discussed later in detail.

It is worthy to note that the findings and conclusions mentioned above were based on laboratory experiment of a relatively small set of samples. More laboratory and field experiments are needed to confirm these conclusions before putting them into engineering application.

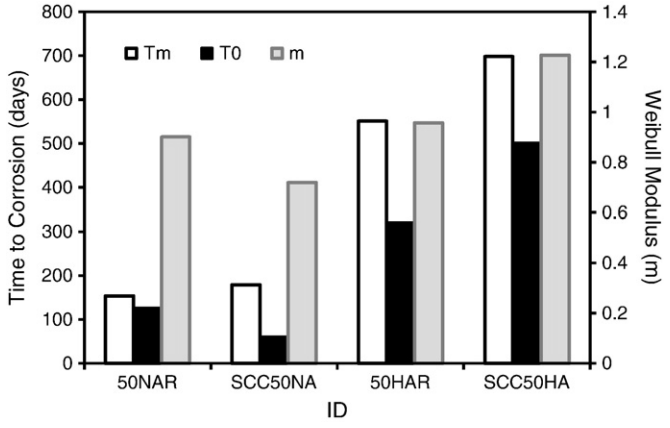

Fig. 10. Plot of mean T_i (T_m), T_0 and m for each mix set.

3.2. Chloride analysis

The data of chloride content are summarized in Table 4 and plotted in Fig. 11. The chloride contents experimentally measured from passive and corrosion active sites of different slab sets increase linearly with the logarithm of time-to-open regardless the different composition and microstructure of the concrete sets. In spite of the large scatters of experimental data, it is still observable that the average chloride content at the active spots are, at a given exposure duration, higher than those at the passive sites. This phenomenon cannot be revealed by the traditional coring sampling approach. If extrapolating the straight lines of chloride content vs. $\log(t_{open})$ to zero time-to-open, we can obtain the minimum duration required for chloride ions reach the rebar surface via mass transport. The data in Fig. 11 indicate that the minimum duration required arriving at the active and passive sites are almost same. However, the exact mechanism to produce the uneven distribution of chloride on the rebar surface is still unknown. Herein, we propose a possible mechanism to interpret this phenomenon. The chloride accumulation at the active spots is faster than that at the passive sites owing to defects presence at the rebar/concrete interface. However, direct experimental evidence is needed to confirm this mechanism.

Fig. 12 shows a plot of chloride data from Table 4 partitioned according to, first, the different concrete sets and, second, active versus passive locations. This plot illustrates that both the SCC and control regular slabs employed high alkalinity cement generally had higher chloride content at corrosion active and passive sites than normal ones. Several mechanisms may be at play that contributed to chloride content difference induced by the cement alkalinity. First and the most important of all, an approximate function [39], as described in Eq. (10), can be used to explain the correlation between chloride content and cement alkalinity.

$$pH = xPM + yPCl + M \tag{10}$$

where the concentration index of hydroxyl anion (pH), metallic cation (PM), and chloride anion (pCl), coefficients x and y, and M is a constant, respectively. From Eq.(10), with the increasing pH, higher chloride content is needed to initiate corrosion of rebar. In other words, the higher pH causes the need for more chloride to be present before a critical level is reached that disrupts the passive film. This is

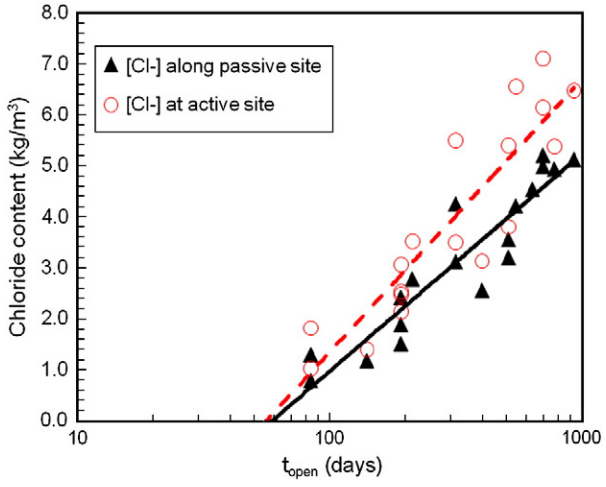

Fig. 11. Chloride content at corrosion active and passive sites respectively as a function of time-to-open for all the slabs.

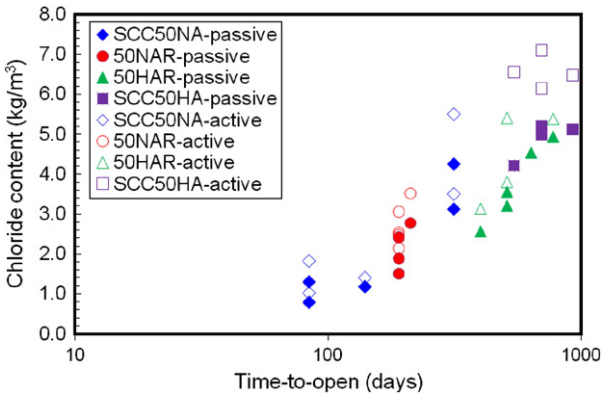

Fig. 12. Chloride content at active and passive sites respectively as a function of time-to-open and concrete mix.

the dominant mechanism. Secondly, a two-fold decrease in the effective Cl^- diffusion coefficient (D_{eff}) [40] has been reported for a Na_2O-equivalent increase in the approximate range involved here. Finally, higher Na_2O-equivalent has been reported to result in reduced Cl^- binding [41], and thus higher availability of free chlorides. This has the opposite effect of the first two mechanisms and apparently plays a relatively minor role.

To further verify the non-uniform chloride content distribution at rebar/concrete interface, the top of rebar trace for slab SCC50HA#1 was sectioned into seven pieces after dissection, as shown in Fig. 13(a). For each piece, chloride content at two spots, one of which at the left side of rebar/concrete interface and the other at the right, was determined using the EDX. The results shown in Fig. 13(b) indicate that the average chloride content was 0.183 concrete wt% (0.732 kg/m^3 for 400 kg/cm^3 concrete) at passive locations along the bar and 0.335 wt.% (1.34 kg/m^3 for 400 kg/cm^3 concrete) at active ones (corresponding to piece #2 in Fig. 13(a) and sites 2 L and 2R in Fig. 13(b)). This confirmed the finding from titrating milling samples that the chloride content at corrosion active site is generally greater than where the steel remained passive. Note that the chloride contents in Fig. 13(b) are lower than Table 4 and Fig. 11, which is due to chloride content derived from different approaches (EDX spectrum for the former and chemical titration for the latter).

3.3. Air void analysis

The results of air void analysis are provided in Fig. 14. Fig. 14(a) and (b), respectively, illustrates the cumulative number and percentage of air voids as a function of void diameter.

Fig. 14(a) shows that the number of air voids at the rebar/concrete interface followed the order of SCC50NA ≫ SCC50HA > 50NAR > 50HAR. This is similar to the order of air content in these concrete mixes measured in the plastic state, 7.6% > 6.6% ≫ 3.1% ≈ 3.3%, as shown in Table 3. It is reasonable to attribute more air voids at the rebar/concrete interface and air content throughout the concrete matrix of SCC concretes, relative to the regular PCC mixes, to the addition of specific superplasticizer. This conclusion may differ from the findings in literature [22,42] since different types or amounts of superplasticizers were used. It can be found that SCC50NAR shows maximum air content in concrete and air void amount at the rebar/concrete interface. These factors facilitate the rapid accumulation of deleterious Cl^- ions and dissolved oxygen at the rebar/concrete interface, especially at the defect (e.g., air void) locations, and further result in higher risk for earlier corrosion initiation.

Fig. 14(b) shows that, regarding big voids (greater than 2.5 mm in diameter), there is only a minor difference for all sets; whereas a greater percentage of small voids (less than 1.0 mm in diameter) exist at the SCC rebar/concrete interface. Regarding the impact of air void size distribution on rebar corrosion initiation, it was revealed [24] that void gap formation under reinforcement greatly increased the risk of rebar corrosion whereas the presence of smaller defects did not show significant impact. A laboratory investigation [25] also indicated that entrapped air voids with diameter ≥2.5 mm at the rebar/concrete interface facilitated the corrosion initiation of steel rebar whereas air voids with diameter <2.5 mm (typical size range of entrained air voids) seemed to be irrelevant to C_{th} and T_i.

These findings can be used to explain why rebars in SCC50HA slabs exhibited better corrosion resistance than those in 50HA. Although more air voids exist at the SCC50HA rebar/concrete interface, there is almost no difference in their big void amount, which facilitates chloride accumulation and rebar corrosion initiation. However, for rebar embedded in normal alkalinity concrete, even though a relatively small percentage of big voids was shown at the SCC50NA rebar/concrete interface, the amount of big void is still more than that of 50NAR owing to much higher total void amount for SCC50NA. Therefore, it is reasonable for SCC50NA to indicate higher risk for earlier corrosion initiation and scatter T_i value shown in Fig. 9. Since no analysis was conducted to directly relate air void location/size and rebar corrosion initiation spot, it is difficult to discern the higher risk for earlier corrosion initiation of SCC50NAR resulted from relatively small or large air voids.

The specific mechanism related to how the air voids at the rebar/concrete interface facilitate the corrosion initiation of rebar is unclear, presumably involving an active–passive electrochemical cell between the concrete-covered steel and the contiguous air void(s) where more dissolved oxygen and free chlorides are available. It can be reasoned that concrete with a relatively high air void content at the steel/concrete interface should have lower C_{th} and T_i values than concrete

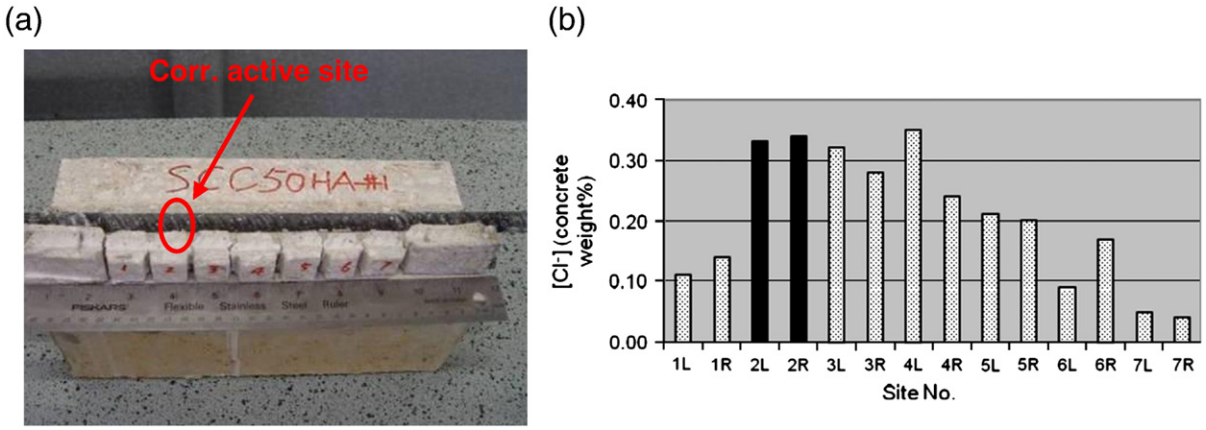

Fig. 13. A dissected SCC50HA slab (a) and the EDX-derived chloride content profile along the top rebar trace (b), once corrosion had initiated.

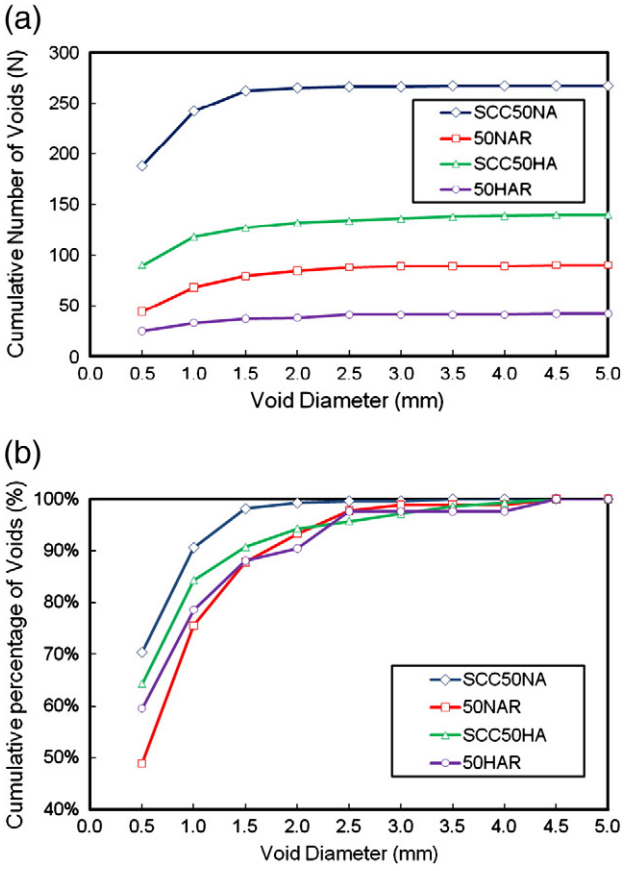

Fig. 14. Cumulative number (a) and cumulative percentage (b) of air voids along rebar atop as a function of void diameter for all slab types.

with less air voids, provided that other relevant factors of the two concrete mixes are comparable. This assumption is well correlated to results acquired from this study and published literature [24–28].

4. Conclusions

This work studied time-to-corrosion (T_i) of reinforcement in concrete and chloride threshold content (C_{th}) for seemingly identical reinforced ASTM G109 SCC using regular concrete slabs as control. The following conclusions can be drawn:

1) Experimental results confirmed that T_i and C_{th}, the two service life determinants of reinforced concrete, should be treated as distributed parameters.
2) Based on Weibull analysis, results indicate that corrosion initiation of rebar embedded in SCC is dependent on cement alkalinity and superplasticizer. Rebar, embedded in high alkalinity cement SCC, exhibits better corrosion resistance expressed as extended T_i (3.6 to 3.9 times of their normal alkalinity counterparts) and higher C_{th}. However, regarding rebar embedded in normal alkalinity cement SCC, scattered T_i and C_{th} illustrated that high risk of earlier corrosion initiation exists, compared with rebar in regular concretes. This conclusion needs to be further confirmed with more laboratory and field tests.
3) It is believed that the addition of specific superplasticizer, interplaying with other factors, improves corrosion resistance of rebar in high alkalinity cement SCC (1.6 times of its normal alkalinity counterpart); whereas, for rebar in normal alkalinity cement SCC, air void amount and size distribution analysis reveal that more voids (defects) produced at the rebar/concrete interface ultimately led to higher risk of earlier corrosion initiation.
4) A new sampling method, milling powder from corrosion active and passive sites at the rebar/concrete interface, for C_{th} determination was adopted. Chloride content at corrosion active site was found to be greater than that at the passive site, and the results of EDX analysis confirm this conclusion.

Acknowledgements

The authors would like to acknowledge the financial support of this research provided by the Florida Department of Transportation (FDOT) and the Federal Highway Administration (FHWA). The opinions expressed represent those of the authors and not necessarily of the FDOT or FHWA.

References

[1] J.N. Enevoldsen, C.M. Hansson, B.B. Hope, Binding of chloride in mortar containing admixed or penetrated chlorides, Cement Concr. Res. 24 (8) (1994) 1525–1533.
[2] Gjørv, Vennesland, Diffusion of chloride ions from seawater into concrete, Cement Concr. Res. 2 (1979) 229–238.
[3] E. Gjørv, K. Tan, M. Zhang, Diffusivity of chlorides from seawater into high-strength lightweight concrete, ACI Mater. J. 91 (5) (1994) 447–452.
[4] R.F. Stratfull, The corrosion of steel in a reinforced concrete bridge, Corrosion 13 (3) (1956) 173–178.
[5] V.K. Gouda, Corrosion and corrosion inhibition of reinforcing steel, Br. Corros. J. 5 (2) (1970) 198–202.
[6] A.L. Page, N.R. Short, W.R. Holden, The influence of different cements on chloride-induced corrosion of reinforcing steel, Cement Concr. Res. 16 (7) (1986) 79–86.
[7] S. Care, Influence of aggregates on chloride diffusion coefficient into mortar, Cement Concr. Res. 33 (7) (2003) 1021–1028.
[8] C. Andrade, Calculation of chloride diffusion coefficients in concrete from ionic migration measurement, Cement Concr. Res. 23 (3) (1993) 724–742.
[9] Z.P. Bazant, Physical model for steel corrosion in concrete sea structures—application, ASCE J. Struct. Div. 105 (June, 1979) 1155–1166.
[10] C.B. Shin, E.K. Kim, Modeling of chloride ion ingress in coastal concrete, Cement Concr. Res. 32 (5) (2002) 757–762.
[11] A. Boddy, E. Bentz, An overview and sensitivity study of a multi-mechanistic chloride transport model, Cement Concr. Res. 29 (6) (1999) 827–837.
[12] D.A. Hausmann, Steel corrosion in concrete: how does it occur? Mater. Prot. 6 (11) (1967) 19–23.
[13] T. Yonezawa, V. Ashworth, R.P.M. Procter, Pore solution composition and chloride effects on the corrosion of steel in concrete, Corrosion 44 (7) (1988) 489–493.
[14] W. Breit, Critical chloride content—investigations of steel in alkaline chloride solutions, Mater, Corros, 49 (6) (1998) 539–550.
[15] L. Li, A.A. Sagûës, Chloride corrosion threshold of reinforcing steel in alkaline solutions—open-circuit immersion tests, Corrosion 57 (1) (2001) 19–28.
[16] K.Y. Ann, H.-W. Song, Chloride threshold level for corrosion of steel in concrete, Corros. Sci. 49 (11) (2007) 4113–4133.
[17] G.K. Glass, N.R. Buenfeld, The presentation of the chloride threshold level for corrosion of steel in concrete, Corros. Sci. 39 (5) (1997) 1001–1013.
[18] C. Alonso, C. Andrade, M. Castellote, P. Castro, Chloride threshold values to depassivate reinforcing bars embedded in a standardized OPC mortar, Cement Concr. Res. 30 (7) (2000) 1047–1055.
[19] C. Alonso, M. Castellote, C. Andrade Chloride, threshold dependence of pitting potential of reinforcements, Electrochim. Acta 47 (2002) 3469–3481.
[20] H. Yu, W.H. Hartt, Effect of reinforcement and coarse aggregates on chloride ingress into concrete and time-to-corrosion: Part I—spatial chloride distribution and implications, Corrosion 63 (9) (2007) 843–850.
[21] ASTM C876-91 (Reapproved 1999), Standard Test Method for Half-Cell Potentials of Uncoated Reinforcing Steel in Concrete, ASTM International, West Conshohocken, PA, 1999.
[22] H. Yu, R.J. Himiob, W.H. Hartt, Effects of reinforcement and coarse aggregates on chloride ingress into concrete and time-to-corrosion: Part 2: spatial distribution of coarse aggregates, Corrosion 63 (10) (2007) 924–931.
[23] G.E. Monfore, G.J. Verbeck, Corrosion of prestressed wire in concrete, ACI. Mater. J. 57 (5) (1960) 491–497.
[24] T.A. Söylev, R. Francois, Corrosion of reinforcement in relation to presence of defects at the interface between steel and concrete, J. Mater Civil Eng 17 (4) (2005) 447–455.
[25] W.H. Hartt, J. Nam, Effect of cement alkalinity on chloride threshold and time-to-corrosion of reinforcing steel in concrete, Corrosion 64 (8) (2008) 671–680.
[26] S. Assié, G. Escadeillas, V. Waller, Estimates of self-compacting concrete 'potential' durability, Constr. Build. Mater. 21 (10) (2007) 1909–1917.
[27] T.A. Söylev, R. François, Quality of steel-concrete interface and corrosion of reinforcing steel, Cement Concr. Res. 33 (9) (2003) 1407–1415.
[28] J.M. Chi, R. Huang, C.C. Yang, Effects of carbonation on mechanical properties and durability of concrete using accelerated testing method, J Marine Sci. Technol. 10 (1) (2002) 14–20.
[29] H.A.F. Dehwah, M. Maslehuddin, S.A. Austin, Effect of cement alkalinity on pore solution chemistry and chloride-induced reinforcement corrosion, ACI. Mater. J. 99 (3) (2002) 227–235.

[30] B.H. Oh, B.S. Jang, Chloride diffusion analysis of concrete structures considering effects of reinforcing, ACI. Mater. J. 100 (2) (2003) 143–149.
[31] S.C. Kranc, A.A. Sagues, F. P-Moreno, Decreased corrosion initiation time of steel in concrete due to reinforcing bar obstruction of diffusional flow, ACI. Mater. J. 99 (1) (2002) 51–53.
[32] P. Cros, W.H. Hartt, H. Yu, Affects of reinforcement on chloride intrusion into concrete and time-to-corrosion, 16th International Corrosion Congress, Sept 22-26, 2005, Beijing, China, 2005.
[33] E.J. Hansen, V.E. Saouma, Numerical simulation of reinforced concrete deterioration: Part I: chloride diffusion, ACI. Mater. J. 96 (2) (1999) 173–180.
[34] H. Yu, W. H. Hartt, Modeling Corrosion Initiation of Reinforcing Steel in Concrete: Effect of Non-Diffusive Coarse Aggregate, Journal of Composite Materials, in press.
[35] ASTM G109-99, Test Method for Determining the Effect of Chemical Admixtures on the Corrosion of Embedded Steel Reinforcement in Concrete Exposed to Chloride Environment, ASTM International, West Conshohocken, PA, 1999.
[36] Florida Method of Test for Determining Low-Levels of Chloride in Concrete and Raw Materials, Designation FM 5-516, Florida Department of Transportation, Tallahassee, FL, Sept., 1994.
[37] W. Weibull, A statistical distribution function of wide applicability, J. Appl. Mech.-Trans. ASME 18 (3) (1951) 293–297.
[38] J.B. Wachtman, W.R. Cannon, M.J. Matthewson, J.B. Wachtman, W.R. Cannon, M.J. Matthewson, Mechanical Properties of Ceramics, 2nd Edition, Wiley InterScience, 2009, pp. 125–128.
[39] N. Sato, The stability of localized corrosion, Corros. Sci. 37 (12) (1995) 1947–1967.
[40] L. Li, J. Nam, W.H. Hartt, Ex-situ leaching measurement of concrete alkalinity, Cement Concr. Res. 35 (2) (2005) 277–285.
[41] J. Tritthart, Chloride binding in cement II. The influence of the hydroxide content in the pore solution of hardened cement paste on chloride binding, Cement Concr. Res. 19 (5) (1989) 683–691.
[42] V. S. Dubovoy, S. H. Gebler and P. Klieger, Cement-Alkali Level as It Affects Air-Void Stability, Freeze-Thaw Resistance, and Deicer Scaling Resistance of Concrete, R & D Bulletin RD128, 2001.